Journal of Computational Physics 228 (2009) 6361–6375

Contents lists available at ScienceDirect

Journal of Computational Physics

journal homepage: www.elsevier.com/locate/jcp

A conservative level set method for contact line dynamics

Sara Zahedi [a,*], Katarina Gustavsson [a], Gunilla Kreiss [b]

[a] School of Computer Science and Communication, Royal Institute of Technology, 100 44 Stockholm, Sweden
[b] Division of Scientific Computing, Department of Information Technology, Uppsala University, 751 05 Uppsala, Sweden

ARTICLE INFO

Article history:
Received 8 February 2008
Received in revised form 6 March 2009
Accepted 12 May 2009
Available online 6 June 2009

Keywords:
Contact line
Contact angles
Level set method
Conservative method
Two-phase flow

ABSTRACT

A new model for simulating contact line dynamics is proposed. We apply the idea of driving contact-line movement by enforcing the equilibrium contact angle at the boundary, to the conservative level set method for incompressible two-phase flow [E. Olsson, G. Kreiss, A conservative level set method for two phase flow, J. Comput. Phys. 210 (2005) 225–246]. A modified reinitialization procedure provides a diffusive mechanism for contact-line movement, and results in a smooth transition of the interface near the contact line without explicit reconstruction of the interface. We are able to capture contact-line movement without loosing the conservation. Numerical simulations of capillary dominated flows in two space dimensions demonstrate that the model is able to capture contact line dynamics qualitatively correct.

1. Introduction

Accurate modeling and simulations of contact-line movement are of interest in areas like lubrication, oil recovery, and immiscible fluid flow through porous media. Another example is the liquid phase sintering process [1] which is important for industrial operations such as grinding, drilling, and cutting. This process permits the formation of dense, pore-free carbides with superior properties such as high strength, hardness and toughness. An important part of the sintering process is wetting of the liquid onto solid particles. The wetting liquid acts on the solid particles to eliminate porosity and reduce interfacial energy. Simulations can contribute to a better understanding of the liquid phase sintering process and play an important role in the development of cutting tools.

Contact line dynamics is the movement of the intersection line between the interface of two immiscible fluids and a solid surface. An example of such a phenomenon is when a droplet with zero velocity is placed on a solid surface and starts to spread. As the drop spreads, the contact line will move until it reaches an equilibrium state determined by the surface energies of the interfaces involved. The angle between the interface at equilibrium and the solid surface is often referred to as the equilibrium or static contact angle (hereinafter, *the static contact angle*). For a more detailed discussion of this kind of phenomena see [2].

The immiscible and incompressible flow is described by the incompressible Navier–Stokes equations with the surface tension and gravity forces added as source terms. Some representation of the interface separating the two fluids is required, for example a level set function or markers, and an evolution equation for the advection of the interface. At all interior points, the physically correct model is that the interface is advected by the fluid velocity. At contact lines, however, the standard boundary condition for the velocity is no-slip, which means that the contact line cannot move. Most often the no-slip boundary condition is adequate. However, in many cases it is unphysical, which is reflected by the shear stress becoming singular.

* Corresponding author.
E-mail address: sara7@csc.kth.se (S. Zahedi).

0021-9991/$ - see front matter © 2009 Elsevier Inc. All rights reserved.
doi:10.1016/j.jcp.2009.05.043

Also, in molecular dynamics simulations, see for example [3] and references therein, the existence of fluid-wall slipping has been observed. Over the years, various techniques to enable the contact line to move have been presented. A common approach is to allow the contact line to move by introducing a so called slip length [4,5]. However, this technique has difficulties in capturing flows dominated by capillary forces. Typically such flows are driven by a deviation of the contact angle from the static angle.

Another approach was suggested by Jacqmin [6] who used a coupled Cahn–Hilliard/Navier–Stokes formulation consisting of the Navier–Stokes equations coupled to a system of two parabolic equations for the chemical potential and the concentration of one of the fluids. In this model, the interface is modeled as a layer with a continuous transition from one fluid to the other, and the contact line as a small region; the part of the interface layer close to the solid boundary. When the angle of the interface differs from the static angle the contact line moves by a diffusive process on a fast time scale in the small region at the boundary so that the contact angle is adjusted to the static value. The result is a region close to the boundary with high curvature of the interface, and consequently a strong surface tension force. The fact that the interface can move by diffusive processes eliminates the need for modeling fluid slip. A drawback with the model suggested by Jacqmin is that the interface must be highly resolved to achieve accuracy. This formulation has been used to investigate basic wetting phenomena, dominated by capillary forces [7].

Another alternative is to use the mismatch between the dynamic and static contact angles directly to obtain movement of the contact line. This approach has for example been used in volume-of-fluids [8] and level set contexts [9]. In these methods the interface is explicitly reconstructed close to the contact line so that the contact angle takes the prescribed value.

In this paper we focus on capillary dominated flow. We introduce an extension of the conservative level set method presented in [10,11], which is capable of capturing contact line dynamics while keeping the conservation property. We formulate a reinitialization procedure for the level set function which makes us able to control contact angles at solid boundaries. For the velocity we use a no-slip boundary condition. The procedure does not involve explicit reconstruction. It is formulated as a partial differential equation, and the contact line moves by diffusion. Similarly to the work by Jacqmin, a contact line region with high curvature is achieved and the surface tension forces the fluids to move. Compared to methods that use the Cahn–Hilliard/Navier–Stokes formulation, our conservative level set method requires less computational effort since a relatively coarse grid is sufficient to capture the dynamics, at least away from contact lines. In this paper we consider problems in two space dimensions where contact lines become contact points.

The paper is organized as follows. In Section 2 we present the incompressible Navier–Stokes equations for two-phase flow, together with a description of our interface representation. We also introduce the main idea behind our new contact line capturing model and present the new reinitialization. In Section 3, the new technique is tested numerically on a scalar model problem. We discuss how to interpret and choose values for the model parameters. In Section 4, we apply the new model to channel flow and the spreading of a droplet on a flat plate. We show that if the contact point region is sufficiently small, the large scale interface movement is essentially independent of the size of this region. Section 5 contains a summary and a discussion of the results.

2. Mathematical model

The fundamental model of two-phase flow consists of the incompressible Navier–Stokes equations coupled with evolution of the interface. At contact points special treatment is needed to provide a mechanism for interface movement. In this section we will present this model.

2.1. The incompressible Navier–Stokes equations

Assume that a given domain Ω is occupied by two immiscible fluids separated by an interface Γ. The equations describing this immiscible flow are the incompressible Navier–Stokes equations with the contributions of the surface tension and gravity forces added as source terms:

$$(\rho\mathbf{u})_t + \nabla\cdot(\rho\mathbf{u}\mathbf{u}) = -\nabla p + \nabla\cdot(\mu(\nabla\mathbf{u} + (\nabla\mathbf{u})^T)) + \rho g\mathbf{e}_g + \sigma\kappa\mathbf{n}\delta_\Gamma, \tag{1}$$

$$\nabla\cdot\mathbf{u} = 0. \tag{2}$$

Here $\mathbf{u}, p, \rho$, and μ denote velocity, pressure, density, and viscosity, respectively. In general ρ and μ are discontinuous across the interface separating the two fluids. The curvature and normal of the interface Γ are denoted by κ and $\mathbf{n}$, and δ_Γ is a Dirac delta function with support on Γ. Its action on any smooth test function v is given by

$$\int_\Omega \delta_\Gamma v\, d\Omega = \int_\Gamma v\, d\Gamma. \tag{3}$$

The direction of gravitation is denoted by $\mathbf{e}_g, g$ is the gravity, and σ is the surface tension coefficient. Non-dimensionalize by introducing

$$\mathbf{x} = l_{\text{ref}}\mathbf{x}', \quad \mathbf{u} = u_{\text{ref}}\mathbf{u}', \quad t = t_{\text{ref}}t', \quad p = p_{\text{ref}}p', \quad \rho = \rho_{\text{ref}}\rho', \quad \mu = \mu_{\text{ref}}\mu'. \tag{4}$$

Here $t_{\text{ref}}, p_{\text{ref}}, \rho_{\text{ref}}, \mu_{\text{ref}}, l_{\text{ref}}$, and u_{ref} are constant reference time, pressure, density, viscosity, length, and velocity. Omitting the primes we obtain

$$\frac{\rho_{\text{ref}} u_{\text{ref}}}{t_{\text{ref}}}(\rho\mathbf{u})_t + \frac{\rho_{\text{ref}} u_{\text{ref}}^2}{l_{\text{ref}}}\nabla\cdot(\rho\mathbf{u}\mathbf{u}) = -\frac{p_{\text{ref}}}{l_{\text{ref}}}\nabla p + \frac{\mu_{\text{ref}} u_{\text{ref}}}{l_{\text{ref}}^2}\nabla\cdot(\mu(\nabla\mathbf{u} + (\nabla\mathbf{u})^T)) + \rho_{\text{ref}}\rho g\mathbf{e}_g + \frac{\sigma}{l_{\text{ref}}^2}\kappa\mathbf{n}\delta(\Gamma), \tag{5}$$

$$\nabla\cdot\mathbf{u} = 0. \tag{6}$$

Suitable choices of the reference time t_{ref} and the reference pressure p_{ref} are

$$u_{\text{ref}}\cdot t_{\text{ref}} = l_{\text{ref}}, \quad p_{\text{ref}} = \rho_{\text{ref}} u_{\text{ref}}^2. \tag{7}$$

Introduce the dimensionless Reynolds, Capillary, and Froude numbers, given by

$$\text{Re} = \frac{\rho_{\text{ref}} u_{\text{ref}} l_{\text{ref}}}{\mu_{\text{ref}}}, \quad \text{Ca} = \frac{\mu_{\text{ref}} u_{\text{ref}}}{\sigma}, \quad \text{and} \quad \text{Fr} = \frac{u_{\text{ref}}}{\sqrt{l_{\text{ref}} g}}, \tag{8}$$

respectively. After dividing (5) by $\frac{\mu_{\text{ref}} u_{\text{ref}}}{l_{\text{ref}}^2}$ we obtain

$$((\rho\mathbf{u})_t + \nabla\cdot(\rho\mathbf{u}\mathbf{u})) = -\nabla p + \frac{1}{\text{Re}}\nabla\cdot(\mu(\nabla\mathbf{u} + (\nabla\mathbf{u})^T)) + \frac{1}{\text{Fr}^2}\rho\mathbf{e}_g + \frac{1}{\text{Re}\,\text{Ca}}\kappa\mathbf{n}\delta(\Gamma). \tag{9}$$

In order to complete the formulation, a representation of the interface and a model for its motion are needed. This will be addressed in the next section.

2.2. An improved level set representation of the interface

Level set representations of the interface in two-phase flow have been used in many flow simulations, see for instance [12] or [13]. The basic idea is that if a level set of a function ϕ_0 defines the interface at $t = 0$, the same level set of the solution to

$$\phi_t + \nabla\cdot(\phi\mathbf{u}) = 0, \quad \phi(\cdot, 0) = \phi_0, \tag{10}$$

defines the interface at later times.

The method proposed in this paper is an extension of the conservative level set method, introduced in [10]. Instead of the signed distance function [12,13] usually used to define the interface, this method uses a regularized indicator function ϕ. The indicator function takes the value 0 in one fluid and the value 1 in the other fluid. The 0.5-level defines the interface. In this way, good conservation properties can be achieved simply by using a conservative discretization. It is essential to use no-flux boundary conditions for ϕ except at in- or out-flow boundaries. The shape of the regularized step function is controlled in a reinitialization step. This step is modeled by a partial differential equation where a non-linear term, resembling a compressive limiter (see [14]), is balanced by diffusion in the normal direction. The normal direction is given by the gradient of the level set function. In the following we introduce a new reinitialization that can be used to also capture contact line dynamics. This is a generalization of the reinitialization procedures used in [10,11].

Our new model mimics the Cahn–Hilliard/Navier–Stokes model in the following way. We have included diffusion of the phases, and this diffusion moves the contact point so that the angle between the interface, defined by the 0.5-level set of ϕ, and the boundary always equals the static contact angle α_s, see Fig. 1. A specific static contact angle corresponds to a specific normal vector to the interface $\mathbf{n}_{\alpha_s}$. Since the gradient of the level set function is related to the normal of the interface by $\mathbf{n} = \nabla\phi/|\nabla\phi|$, the condition on the angle can be formulated as a condition on the gradient. We cannot, however, directly

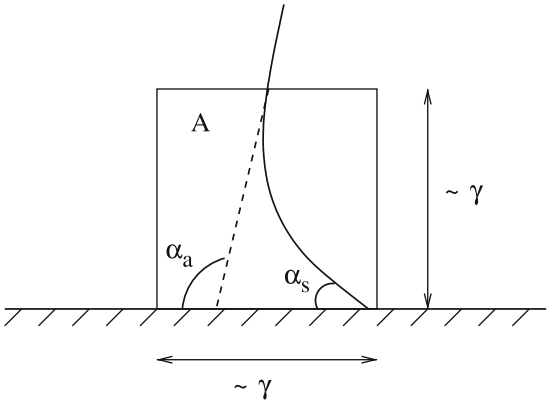

Fig. 1. Definition of different angles.

prescribe the gradient of the level set function at the boundary without creating a flux of ϕ over the boundary that would destroy the conservative properties of the model.

Instead we introduce a regularized normal vector field $\mathbf{n}$, satisfying

$$\tilde{\mathbf{n}} - \nabla \cdot (\gamma^2 \nabla \tilde{\mathbf{n}}) = \frac{\nabla \phi}{|\nabla \phi|}, \quad \mathbf{n} = \frac{\tilde{\mathbf{n}}}{|\tilde{\mathbf{n}}|}, \tag{11}$$

with Dirichlet boundary conditions, $\tilde{\mathbf{n}} = \mathbf{n}_{\alpha_s}$ along solid walls, where $\mathbf{n}_{\alpha_s}$ is the normal corresponding to the static contact angle. The regularization parameter γ should preferably be chosen $\gamma \ll L$, where L is the length of typical features in the problem at hand. The regularized normal vector will have approximately the same direction as the gradient of the unperturbed ϕ, except along the boundary, where a boundary layer with thickness proportional to γ will form. In the boundary layer the regularized normal vector field changes smoothly to the prescribed $\mathbf{n}_{\alpha_s}$. This regularized normal vector field is then used in the reinitialization step in the following fashion:

$$\phi_{\tilde{t}} + \nabla \cdot (\phi(1-\phi)\mathbf{n}) - \nabla \cdot (\varepsilon_n (\nabla \phi \cdot \mathbf{n})\mathbf{n}) - \nabla \cdot (\varepsilon_\tau (\nabla \phi \cdot \mathbf{t})\mathbf{t}) = 0. \tag{12}$$

Here $\mathbf{n}$ is the normalized and regularized gradient of ϕ, satisfying (11), and $\mathbf{t}$ is the tangent, orthogonal to $\mathbf{n}$. Further, ε_n is a diffusion parameter in the normal direction and ε_τ is a diffusion parameter in the tangential direction. The second term in (12) represents compression in the normal direction, while the third models diffusion in the normal direction, and the last term models diffusion in the tangential direction. A balance between the second and the third terms establishes a layer of thickness proportional to ε_n, where ϕ changes from 0 to 1. For the method to be accurate, ε_n must be much smaller than typical geometrical features of the interface. In the original work on the conservative level set method [10] the standard isotropic diffusion was used. This corresponds to choosing $\varepsilon_\tau = \varepsilon_n = \varepsilon$ in Eq. (12). In the subsequent work, presented in [11], $\varepsilon_\tau = 0$. The idea was to avoid unnecessary movement of the 0.5-level set in the tangential direction. However, the tangential diffusion is essential in the contact point region. It ensures that the level set function is constant in the tangential direction. At the boundary this implies that the 0.5-level set forms the prescribed angle to the boundary.

Using this model, the interface should be advected with the fluid velocity everywhere except in the contact point region. There the reinitialization step establishes a boundary layer in ϕ, of thickness proportional to the regularization parameter γ. The angle of the interface (the 0.5-level set of ϕ) to the boundary changes over the boundary layer from the static contact angle α_s to the apparent contact angle α_a. The apparent contact angle is the angle formed between the boundary and the interface away from the contact point region, see Fig. 1. Close to the boundary the curvature of the interface will in general be large if γ is small. As long as the apparent angle remains the same the reinitialization step will ensure that the shape of the interface in the contact point region is constant. This means that the contact point moves with the same speed as the tangential fluid velocity just outside the contact point region (region A in Fig. 1).

We expect the velocity of the contact point to be determined by a balance between surface tension and viscous forces. When the two fluids have the same viscosity the following simple analysis shows that for small γ the speed is essentially independent of γ. Let the dimensionless speed of the contact point be U. Then, since the fluid velocity changes from 0 to U over a layer of thickness proportional to γ, the viscous stress in the tangential direction, in the Navier–Stokes equations (9), is proportional to U/γ^2. The resulting viscous force on A is obtained by integrating over A, yielding $F_{\text{visc}} \sim U$. The term representing surface tension is $\frac{1}{\text{Ca}} \kappa \mathbf{n} \delta(\Gamma)$, with $\text{Ca} = \frac{\mu_{\text{ref}} u_{\text{ref}}}{\sigma}$. The curvature κ depends on the static and apparent angles in some non-trivial way, but scales inversely with γ, that is $\kappa \sim \frac{f(\alpha_a, \alpha_s)}{\gamma}$. Integrating over A yields a tangential force $F_{\text{surface}} \sim \frac{f(\alpha_a, \alpha_s)}{\text{Ca}}$. The two forces, F_{visc} and F_{surface}, must be balanced, yielding $U \sim \frac{f(\alpha_a, \alpha_s)}{\text{Ca}}$. This indicates that at least to lowest order in γ, U is independent of γ. Also note that in the limit $\gamma \to 0$ the shear stress is still singular, but now the singularity is integrable. In the next section these ideas are tested numerically for a model problem.

3. Model problem

In this section numerical tests are performed with the intention to show how different parameters in the new model for the reinitialization, introduced in Section 2.2, influences the level set function ϕ and to give an idea of how they should be chosen. In this section, we are only interested in the contact point region and therefore we only consider the reinitialization process, and we do not solve any advection equation for ϕ. We recall that the reinitialization process is governed by Eqs. (11) and (12).

In this section we model a contact point region of a real problem, scaled so that the curvature of the interface away from the contact point is small compared to unity. Also, by a simple scaling argument it is clear that only the ratio between the modeling parameters is important for the shape of the interface in the contact point region. We therefore keep ε_n fixed in this section, and vary only γ and ε_τ.

Throughout this section the computational domain is $\{(x, y) : 0 \leqslant x \leqslant 2, 0 \leqslant y \leqslant 2\}$. Initially

$$\phi(x, y) = \frac{1}{1 + e^{\frac{1-x}{\varepsilon_n}}},$$

which gives an interface at $x = 1$ normal to the x-axis. Thus, the normal at the interface $\frac{\nabla \phi}{|\nabla \phi|} = (1, 0)$, corresponding to an apparent contact angle of 90°. With this normal, Eq. (11) can be solved analytically for the regularized normal vector field.

Let $\tilde{\mathbf{n}} = (n_1, n_2)$ be the component of the normal vector in the x- and y-direction respectively. Then

$$n_1(y) = c_1 e^{y/\gamma} + c_2 e^{-y/\gamma} + 1, \tag{13}$$

$$n_2(y) = c_3 e^{y/\gamma} + c_4 e^{-y/\gamma}, \tag{14}$$

where the constants c_1, c_2, c_3, and c_4 are given by the boundary conditions,

$$n_1(0) = \sin(\alpha), \quad \frac{dn_1}{dy}(2) = 0,$$

$$n_2(0) = \cos(\alpha), \quad \frac{dn_1}{dy}(2) = 0.$$

Here α is the prescribed contact angle of the interface at the contact point. In this work we prescribe the contact angle to be equal to the static contact angle α_s.

The reinitialization equation (12) is discretized on a uniform mesh with grid size h in both x- and y-directions using a conservative second order finite difference scheme. On the boundaries, the numerical flux functions are set to zero. For the time stepping we use a second order Runge–Kutta scheme and for stability reasons, the time step is chosen as $\Delta t = h^2/(2(\varepsilon_n + \varepsilon_\tau))$. The reinitialization equation is solved until the relative residual of ϕ, $\frac{\|\phi^{n+1} - \phi^n\|_2}{\|\phi^n\|_2} \leqslant 10^{-5}$, which we consider to be the steady solution. In this section we will use a mesh size of $h = 0.005$ in all numerical experiments. We have performed mesh convergence studies which showed that the value of h chosen here is sufficiently small for the computations in this section to be well resolved.

3.1. The regularization parameter γ

We will now investigate how the parameter γ affects the contact point region. To study the influence of γ on the level set function ϕ, the reinitialization equation (12) is solved with a regularized normal vector field for different values of the parameter γ. The other parameters are kept fixed at $\varepsilon_n = 8h$ and $\varepsilon_\tau = 6\varepsilon_n$.

The 0.5-level set of ϕ defining the interface after the reinitialization is shown in Fig. 2 for different values of γ and for a prescribed contact angle of $\alpha_s = 45^\circ$. We can clearly see the influence of γ on the interface. A boundary layer proportional to γ is formed in the reinitialization process. In this layer the normal of the interface varies smoothly from the prescribed normal at $y = 0$ to the gradient of the unperturbed level set function ϕ. Reinitialization with small values of γ will produce an interface with large curvature. Also, the position of the point where the 0.5-level set intersects the boundary $y = 0$ depends on the value of γ. The contact angle at steady state comes closer to the prescribed angle when γ is increased.

In Fig. 3 we show how the contact angle changes with time for the different values of γ. Starting from 90° the contact angle decreases with time towards the prescribed static contact angle. We can see a similar behavior for all four values of γ and that γ has a small impact on the obtained contact angle.

To conclude this section, γ should be small, in the order of ε_n, so that the contact point region does not become a substantial part of the domain. However, a smaller γ generally gives larger curvature. The mesh size h must be chosen small enough to resolve the curvature.

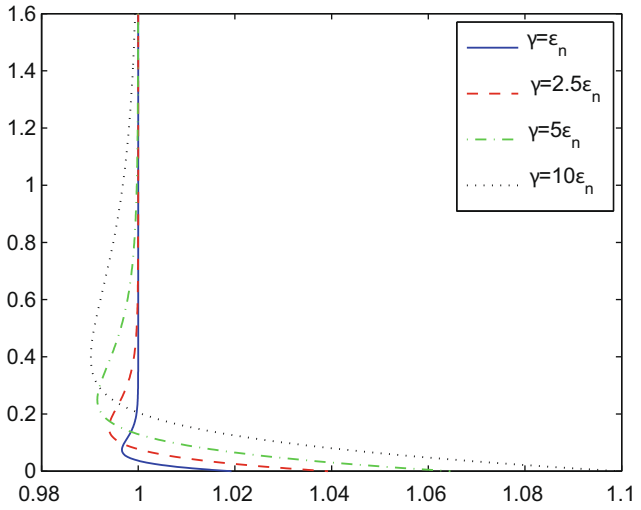

Fig. 2. The steady 0.5-level set of ϕ for different values of γ. Here $\varepsilon_n = 8h, \varepsilon_\tau = 6\varepsilon_n$ and $\alpha_s = 45^\circ$. The contact angle of the interface at the boundary where the 0.5-level set intersects $y = 0$, has reached approximately 50°, 49°, 48°, and 46° for $\gamma/\varepsilon_n = 1, 2.5, 5,$ and 10, respectively.

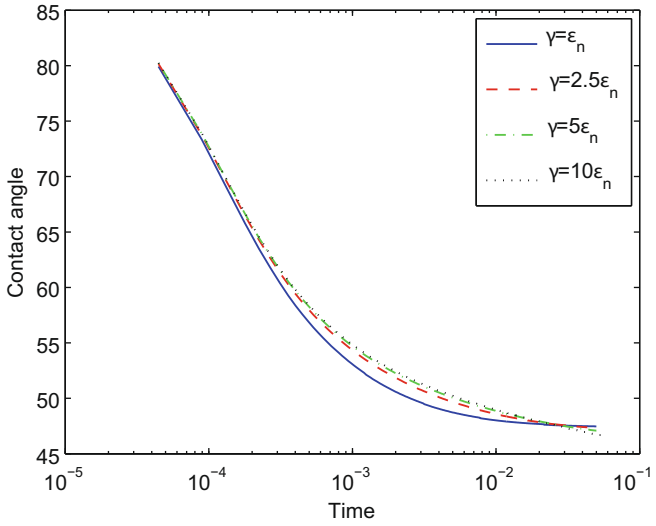

Fig. 3. The contact angle as a function of time in the reinitialization process for different values of γ. Here $\varepsilon_n = 8h, \varepsilon_\tau = 6\varepsilon_n$ and $\alpha_s = 45^\circ$.

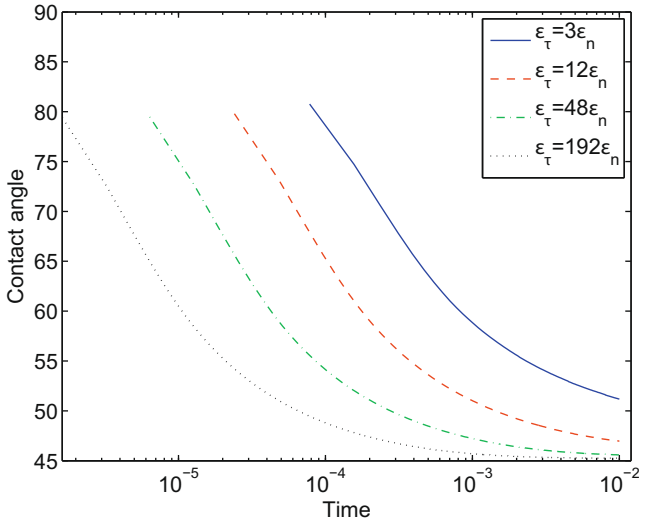

Fig. 4. Contact angle as a function of time in the reinitialization process for different values of ε_τ. Here we have used fixed values of $\varepsilon_n = 8h$ and $\gamma = 2.5\varepsilon_n$ and $\alpha_s = 45^\circ$. Note that for the smaller values of ε_τ, the angle presented here has not yet reached the steady value. In Fig. 6 you can see how close the steady state angle comes to the prescribed value for different ε_τ-values.

3.2. The tangential diffusion parameter ε_τ

Diffusion in the tangential direction, given by the tangential diffusion parameter, ε_τ, is essential for the ability of the interface to form the prescribed angle to the boundary. To study the influences of ε_τ on the 0.5-level set and more specifically on the angle of the interface to the boundary we have performed simulations with different values of ε_τ for fixed values of $\varepsilon_n = 8h$ and $\gamma = 2.5\varepsilon_n$. The prescribed static angle is $\alpha_s = 45^\circ$.

In Fig. 4 we see that the value of the tangential diffusion has a large impact on the contact angle and as ε_τ increases, the contact angle converges faster towards the static angle α_s. As the tangential diffusion increases, the shape of the foot converges, as can be seen in Fig. 5. However, a larger value of ε_τ will also affect the level set function ϕ away from the contact point region.

The same numerical tests were made also for a prescribed static contact angle of $\alpha_s = 25^\circ$. The behavior of the contact angle is essentially the same. As the tangential diffusion increases the contact angle converge faster towards the static angle. However, larger values of the tangential diffusion is needed when the difference between α_s and the initial contact angle is large. This can be seen in Fig. 6 where the contact angle of the 0.5-level set at steady state is presented as a function of the

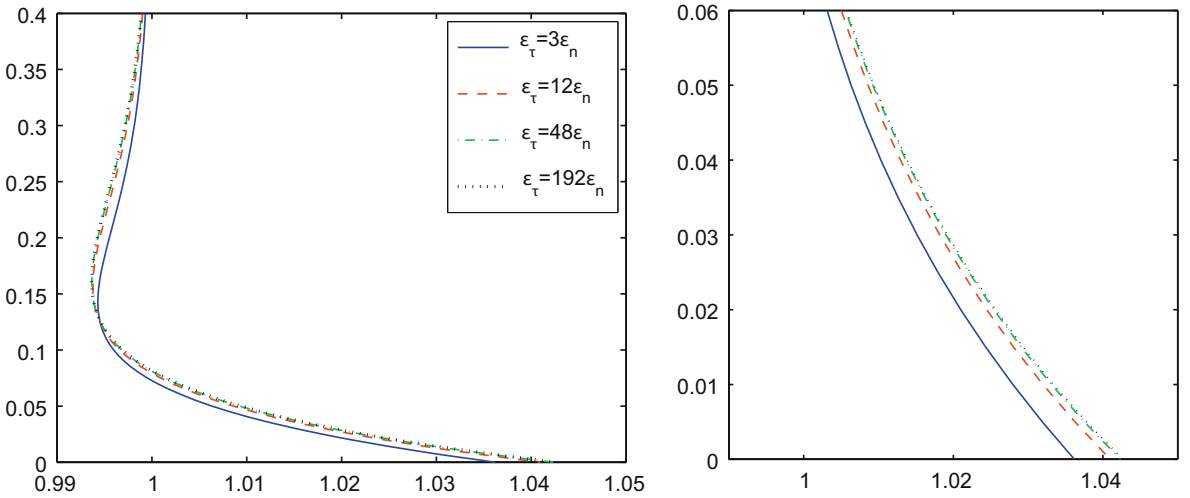

(a) The foot region (b) Close up at the boundary

Fig. 5. The steady 0.5-level set of ϕ for different values of ε_τ. Here $\varepsilon_n = 8h$, $\gamma = 2.5\varepsilon_n$ and $\alpha_s = 45^\circ$.

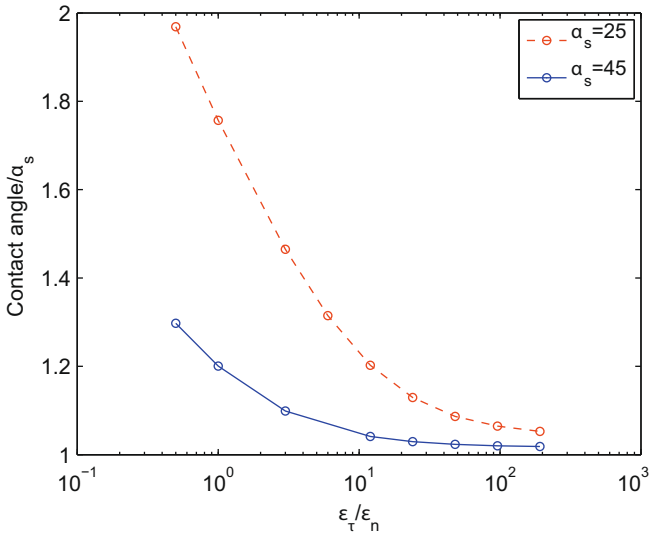

Fig. 6. The contact angle normalized by the static angle as a function of tangential diffusion, ε_τ, for two different values of α_s. Here $\varepsilon_n = 8h, \gamma = 2.5\varepsilon_n$.

ratio $\varepsilon_\tau/\varepsilon_n$, for $\alpha_s = 45^\circ$ and 25°. We have found that varying ε_τ or ε_n without changing their ratio does not affect the obtained contact angle. This means that an improved convergence towards the static contact angle can be obtained either by increasing ε_τ or decreasing ε_n while keeping the other one fixed. This exposes a trade off. On one hand, we do not want to increase ε_τ too much since a large ε_τ will affect the level set function ϕ also in regions away from the foot region. On the other hand, decreasing ε_n requires a finer mesh. A solution could be to let ε_τ vary with the distance from the boundary. In this way we would get tangential diffusion only in the foot region.

3.3. Conclusions

A general conclusion from the results presented here is that larger values of γ and ε_τ result in contact angles closer to the prescribed angles. The value of the regularization parameter γ does not have as large effect on the contact angle as the tangential diffusion parameter, ε_τ, but γ has a larger impact on the size of the foot region.

Also, at a fixed set of parameters, the discrepancy between the prescribed contact angle α_s and the angle of the interface at the boundary, increases as the difference between α_s and the initial contact angle increases. Larger values of ε_τ are then needed in order to obtain the correct angle, however at the cost of the parameters influencing a larger region. A remedy for this could be to add tangential diffusion only in the contact point region.

An improved convergence towards the static contact angle can also be obtained by decreasing ε_n. This would, however, require a finer mesh.

4. Application

In this section we discuss the numerical treatment and results for two types of applications: channel flow and droplets on flat plates. Both involve two immiscible fluids and moving contact lines. In the channel flow and one of the droplet on a flat plate applications, capillary effects dominate. In the second droplet on a flat plate application, we also see the effect of inertia. The proposed model is used to simulate the contact line dynamics.

4.1. Numerical treatment

The numerical simulations were carried out using FemLego, a parallel finite element code for the solution of partial differential equations [18]. All equations were discretized in space using piecewise linear functions. As in [11], we solve the Navier-Stokes equations by using a projection method [15] with an added pressure stabilization term. The surface tension effect is treated as a force, $F = \sigma\kappa\mathbf{n}\delta_\Gamma$ added to the Navier–Stokes equations. We have implemented two approaches to model the surface tension force. In the first approach, the singular surface tension force is smoothed out over a finite thickness and is given by $F = \sigma\kappa\nabla\phi$ as proposed by Brackbill et al. [16]. In the second approach, the singular surface tension force is evaluated through a line integral along the interface Γ as suggested by Tornberg and Engquist [17]. Our model works well together with both approaches. However, in the first approach the delta function δ_Γ is regularized and if part of the regularization zone ends up outside the computational domain the accuracy will usually be lost. Therefore evaluation of a line integral may be favorable when the interface is close to a boundary.

At contact points diffusion of ϕ tangential to the interface is essential. The diffusion can be added in the reinitialization equation (12), or in the advection equation. In each time step the reinitialization equation (12) is solved until the relative residual of ϕ, $\frac{\|\phi^{n+1}-\phi^n\|}{\|\phi^{n+1}\|} \leqslant 10^{-5}$, which we consider to be the steady state solution. As in [11] we use a second order semi-implicit discretization in time. Usually two reinitialization steps are required. However, in case a large change of the contact angle is needed, more steps are required to reach steady state.

4.2. Capillary dominated channel flow

Consider two fluids with the same density and viscosity, in a two-dimensional channel initially separated by an interface, normal to the channel, without curvature. Thus, the initial apparent contact angle is $\alpha_a = 90^\circ$. We assume that the static contact angle α_s is smaller than 90°. Clearly the initial condition is not a steady state solution. In the absence of an outer pressure gradient or prescribed flux, the only driving force is the capillary effect at the channel walls, which will move the interface to the right.

If the densities and viscosities of the two fluids are of similar size we expect that after an initial, transient process, the interface will move at a constant speed U. We expect the interface to consist of an interior part with curvature $\kappa_a = 2\cos(\alpha_a)$, and two small sections close to the walls with curvature $\kappa \sim \frac{f(\alpha_a-\alpha_s)}{\gamma}$, where f is some smooth function.

4.2.1. Computations

In this subsection we present computations that demonstrate the qualitative behavior of our model. In the computations we consider a channel of non-dimensional length 1 or 2 and width 1. The Capillary number and the Reynolds number are set to unity. At the channel walls we prescribe zero velocity, i.e. no-slip, and the flux of the level set function is set to zero. The normal vectors at the lower and upper walls are prescribed so that the contact angles equal the static contact angles. At the inlet and outlet we use vanishing tangential velocity, vanishing normal derivative of the normal velocity, and Dirichlet conditions for the level set function and the pressure. Throughout this subsection we use $h = \Delta x = \Delta y = 0.01, \Delta\hat{t} = \Delta t = 0.05$, and $\varepsilon_\tau = \varepsilon_n = \varepsilon$.

In Figs. 7 and 8 we see results for a case with static contact angle $\alpha_{s_1} = 45^\circ$ at the upper channel wall, and static contact angle $\alpha_{s_2} = 90^\circ$ at the lower wall. In this computation we used $\varepsilon = 2.5h$ and $\gamma = 3\varepsilon$. As expected, the capillary forces at the upper wall exhort a pull which sets the fluid into motion. In Fig. 7(a) we see how the interface (the 0.5-level set of ϕ) develops over time. In Fig. 7(b) a detail of the interface close to the upper wall at an early stage is shown. The angle between the interface and the upper wall is somewhat larger than 45°. Two representative velocity fields are plotted in Fig. 8. The interface develops into a steady shape after an initial transient period of time. Here we note that away from the interface the velocity field approaches the standard pipe flow parabola.

In Fig. 9 we have plotted results when the static angle is the same at the upper and the lower channel walls, $\alpha_{s_1} = \alpha_{s_2} = 45^\circ$ and $\alpha_{s_1} = \alpha_{s_2} = 25^\circ$, respectively. In these computations the channel length is 2, and we used $\varepsilon = 0.05$, $\gamma = 0.025$. Also in these cases, after a transient period, a steady shape develops which moves at a constant speed. As expected, the interface moves faster when the static contact angle is smaller. In Fig. 10 we have plotted the velocity field, the pressure field, and the level set function at $t = 10$ for the case $\alpha_{s_1} = \alpha_{s_2} = 25^\circ$.

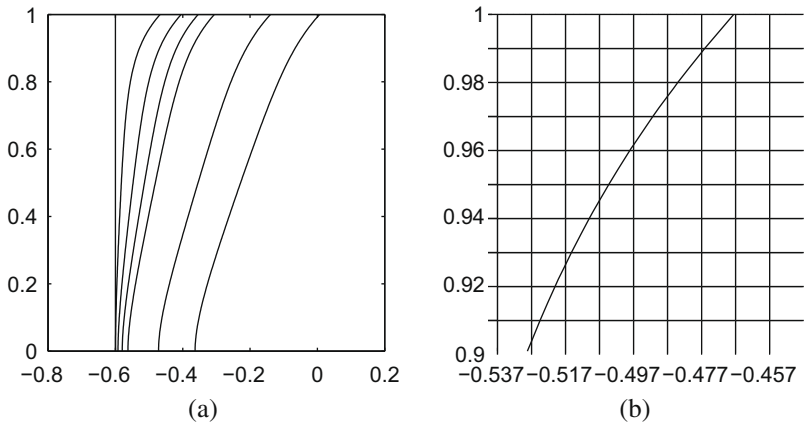

Fig. 7. Capillary dominated channel flow. The static contact angles at the upper and lower wall are 45° and 90° respectively. (a) The location of the interface, represented by the 0.5-level set of ϕ, at $t = 0, 1, 2, 3, 4, 8$, and 12. (b) Detail of the 0.5-level set of ϕ close to the upper wall at $t = 1$ with the grid.

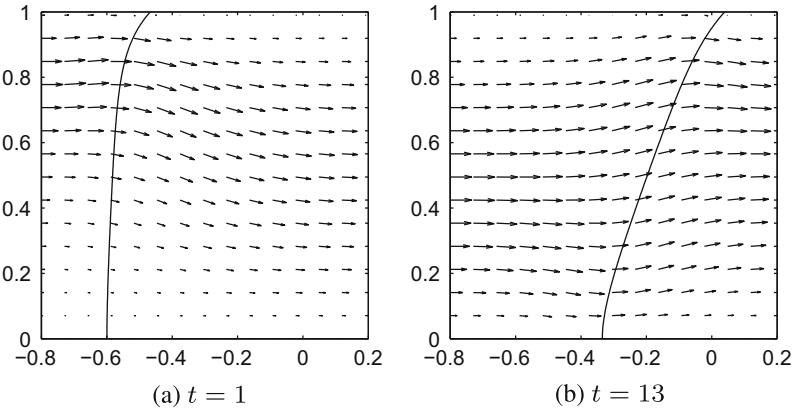

Fig. 8. The same capillary dominated channel flow as in Fig. 7. The normalized velocity field at two different times, $t = 1$ and 13.

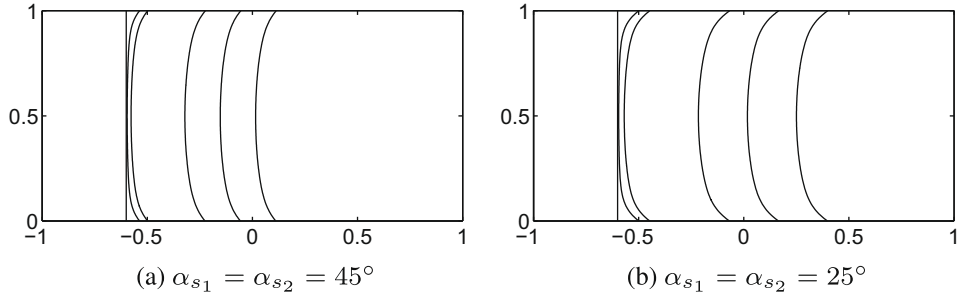

Fig. 9. The location of the interface (the 0.5-level set of ϕ) at $t = 0, 1, 2, 10, 15$, and 20. The angles at the upper and the lower channel walls are $\alpha_{s_1} = \alpha_{s_2} = 45°$ in Panel (a) and $\alpha_{s_1} = \alpha_{s_2} = 25°$ in Panel (b).

4.2.2. Convergence studies

In Section 3 we saw that the shape of the contact point region, or the foot region, is determined by the relation between the model parameters γ, ε_τ, and ε_n. The purpose of this section is to show that when the size of the foot region is decreased, at some point, the movement of the interface is no longer affected.

To obtain an angle which deviates at most 10% from the desired static contact angle of 45° we use the suggested ratios between the modeling parameters, $\varepsilon_\tau/\varepsilon_n = 3$, $\gamma/\varepsilon_n = 2.5$, see Fig. 6. The time step is $\Delta t = 10^{-3}$ and $\Delta\hat{t} = \frac{h^2}{\varepsilon_n+\varepsilon_\tau}$. Initially the interface is a straight line at $x = -0.3$.

In the first set of computations the resolution is set to $h = 0.0025$. Fig. 11 shows the results at $t = 3$ for three values of ε_n, differing by successive factors of two. For the smallest value of ε_n we have $\varepsilon_n = 3\sqrt{2}h = 0.0106$.

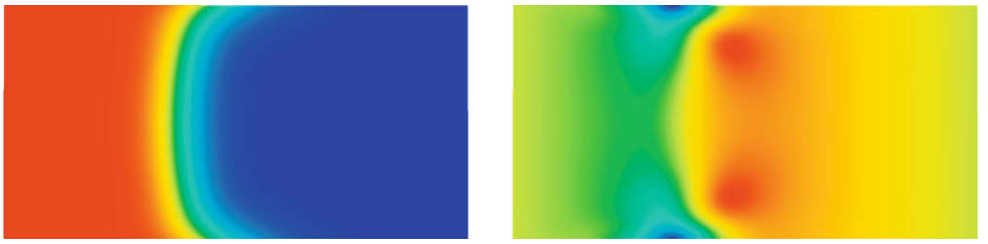

(a) The level set function, ϕ (b) Pressure field

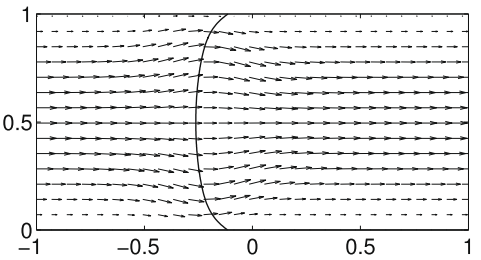

(c) Normalized velocity field

Fig. 10. Solution at $t = 10$ for $\alpha_{s_1} = \alpha_{s_2} = 25^\circ$.

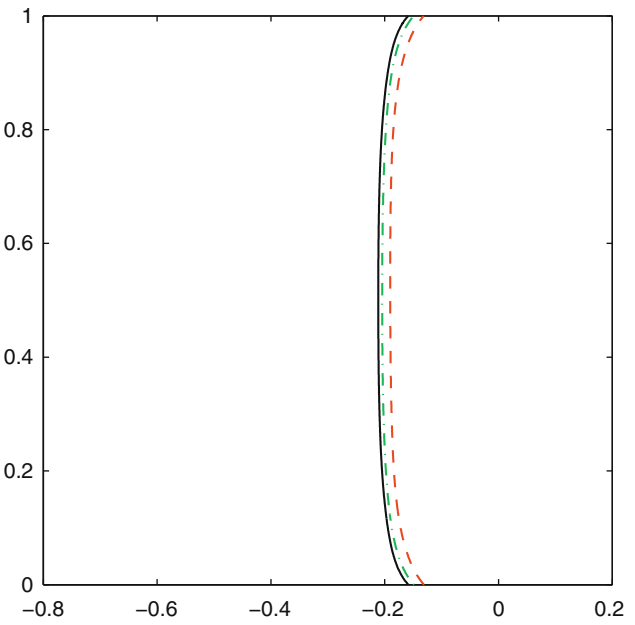

Fig. 11. Comparison between the 0.5-level set of ϕ at $t = 3$ for $\alpha_{s_1} = \alpha_{s_2} = 45^\circ$. The width of the interface $\varepsilon_n = 0.0106$, the diffusion parameter $\varepsilon_t = 3\varepsilon_n$, and the regularization parameter $\gamma = 2.5\varepsilon_n$ were all scaled with 2 and 4. The mesh resolution is fixed to be $h = 0.0025$. The contour furthest to the right corresponds to the largest parameter values.

We compute the order of convergence by comparing the position of 400 points along the interface at $t = 1, 2, 3, 4, 5$ for different values of the modeling parameters. Let x_i^ε be the x-coordinate of the interface at $y = y_i$ at a particular time for $\varepsilon_n = \varepsilon = 0.0106$. If we assume the position of the interface to depend on ε as

$$x_i^\varepsilon = x + \alpha\varepsilon^p + \mathcal{O}(\varepsilon^{p+1}), \tag{15}$$

we can estimate the convergence rate p from $x_i^\varepsilon, x_i^{2\varepsilon}$, and $x_i^{4\varepsilon}$ by

$$p \approx \log\left(\frac{\sum_{i=1}^{400}|x_i^{4\varepsilon} - x_i^{2\varepsilon}|}{\sum_{i=1}^{400}|x_i^{2\varepsilon} - x_i^{\varepsilon}|}\right) \Big/ \log(2). \tag{16}$$

Table 1
Convergence rate for the interface position at different times. The first row shows the convergence rates when the model parameters $\varepsilon_n, \varepsilon_\tau$, and γ are decreased. The mesh size h is fixed. The second row shows the convergence rates when the mesh size is decreased. The time step in the reinitialization $\Delta\hat{t} = \frac{h^2}{\varepsilon_n+\varepsilon_\tau}$.

	$t=1$	$t=2$	$t=3$	$t=4$	$t=5$
$\varepsilon \to 0$	1.0912	1.0401	1.003	0.9702	0.9616
$h \to 0$	0.6831	0.9295	1.1576	1.3031	1.0696

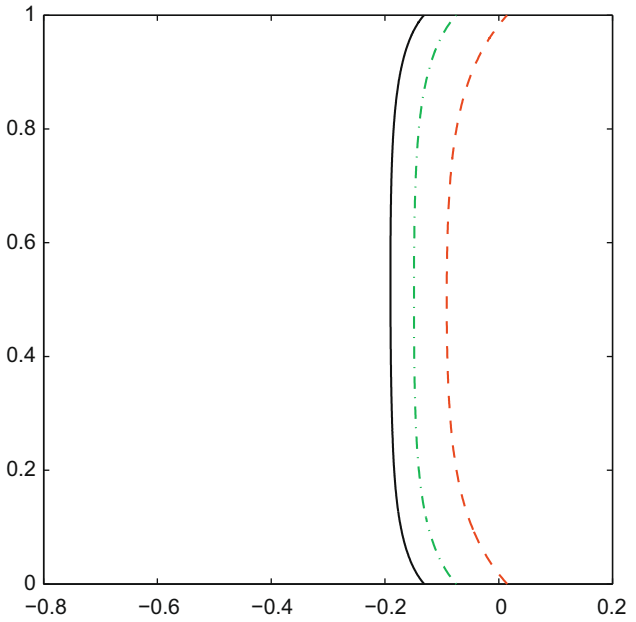

Fig. 12. Comparison between the 0.5-level set of ϕ at $t = 3$ for $\alpha_{s_1} = \alpha_{s_2} = 45^\circ$. Varying the mesh resolution: $h = 0.0025, 0.0025\sqrt{2}, 0.005$ but keeping all the other parameters fixed.

The results of such computations for $t = 1, 2, 3, 4, 5$ indicate linear convergence for the position of the interface, see Table 1. We also obtained linear convergence in the velocity. The velocity was computed by the difference between the x-coordinates of the interface at $y = 0.5$ at two different times divided by the time difference.

In the second set of computations we varied the resolution in space, but kept the modeling parameters fixed with $\varepsilon_n = 4\varepsilon = 0.0424, \varepsilon_\tau/\varepsilon_n = 3$, and $\gamma/\varepsilon_n = 2.5$. In Fig. 12 the results for three values of h, differing by successive factors of $\sqrt{2}$, are plotted. Convergence rates are computed as above, and indicate linear convergence, see Table 1.

4.3. Droplet on a flat plate – capillary dominated

We consider here a two-dimensional droplet with diameter l_{ref}, density ρ_{ref}, and viscosity μ_{ref}, lying on a solid surface surrounded by another liquid with the same density and viscosity. The static contact angle is $\alpha_s = 25^\circ$. Capillary effects dominate and gravity is neglected. We will simulate how this droplet wets the surface. This wetting phenomenon was previously studied using a phase field method by Villanueva and Amberg [7].

Experiments with gas/liquid/solid systems where the viscosity ratio $\lambda = \frac{\mu_M}{\mu_L}$ ranges from 10^{-5} to 10^{-8} has been performed by Hoffman [19]. The experiments show that the apparent contact angle is primarily a function of the capillary number Ca^*. Later Cox [20] presented a more general analysis of the dynamics of wetting. We will compare our results with data from Cox's theory and the phase field simulation.

4.3.1. Cox's theory

Given two immiscible fluids with viscosity ratio λ, Cox's theory states that at a leading order in Ca^*,

$$g(\alpha_D, \lambda) - g(\alpha_s, \lambda) = \text{Ca}^* \ln(\delta^{-1}), \tag{17}$$

where α_D is the macroscopic dynamic contact angle, α_s is the static contact angle, δ is a small constant, and the function $g(\alpha, \lambda)$ is given by

$$g(\alpha, \lambda) = \int_0^\alpha \frac{d\alpha}{f(\alpha, \lambda)}, \tag{18}$$

where

$$f(\alpha,\lambda)=\frac{2\sin\alpha(\lambda^2(\alpha^2-\sin^2\alpha)+2\lambda(\alpha\pi-\alpha)+\sin^2\alpha)+(\pi-\alpha)^2-\sin^2\alpha}{\lambda(\alpha^2-\sin^2\alpha)((\pi-\alpha)+\sin\alpha\cos\alpha)+((\pi-\alpha)^2-\sin^2\alpha)(\alpha-\sin\alpha\cos\alpha)}. \tag{19}$$

It is interesting to note that when Hoffman plotted the observed macroscopic contact angle α_D versus the capillary number Ca^* plus a shift he observed that his experimental results fell on a single curve. He did not, however, provide an explicit mathematical form for the function $\alpha_D(\mathrm{Ca}^*)$. Later Cox showed good agreement between his formula in (17) with $\delta=10^{-4}$ and Hoffman's curve for all values of α_D, except those very close to 180°. We have confirmed that a value of $\delta\approx 10^{-4}$ minimizes the sum of squares of the relative difference between the contact-line speeds Ca^* obtained from the experiments by Hoffman using silicone fluid with $\lambda=0$ and $\alpha_s=0$ and those obtained from Cox's theory. In the following we will use $\delta=10^{-4}$.

4.3.2. Computations

The computational domain is in non-dimensional coordinates $\{(x,y): -2\leqslant x\leqslant 2, 0\leqslant y\leqslant 2\}$ and the initial drop is symmetric around $x=0$ and has non-dimensional radius $r=0.5$. At initial time the drop is in contact with the solid wall at an angle of 156°. The Reynolds number $\mathrm{Re}=\frac{\rho_{\mathrm{ref}}u_{\mathrm{ref}}l_{\mathrm{ref}}}{\mu_{\mathrm{ref}}}=1$ and the Capillary number $\mathrm{Ca}=\frac{2\sqrt{2}\mu_{\mathrm{ref}}u_{\mathrm{ref}}}{3\sigma}=1$. The simulation of the wetting is performed using a mesh consisting of regular triangles with 270×135 nodes and a time step $\Delta\hat{t}=\Delta t=0.0011$. The liquid–liquid interface (the 0.5-level set of ϕ) is advected by solving the advection equation (10) with a diffusion term equal to 0.0011. In the reinitialization described in Eq. (12) the diffusion parameter in the normal direction is set to $\varepsilon_n=4.5h$ where h is the mesh size and the diffusion parameter in the tangential direction is set to $\varepsilon_\tau=0$. The regularization parameter $\gamma=2.5\varepsilon_n$. The boundary condition for the regularized normal vector field, Eq. (11), is set to

$$\mathbf{n}|_{y=0}=(-\mathrm{sign}(x)0.4226,-0.9063)$$

aiming for a contact angle of 25° at the wall $y=0$. At the other boundaries we use homogeneous Neumann conditions. The model parameters were chosen to keep the contact point region small without having to use a very fine mesh. However, we recall from Section 3 that the actual contact angle will be larger than the static contact angle of 25° with our choice of model parameters. We measure the dynamic contact angle that the liquid–liquid interface makes with the solid surface at the inflexion point of the foot as illustrated in Fig. 13. The wetting speed is given by dividing the difference in position of the intersection point (see Fig. 13) at two successive times by the time difference.

In Fig. 14 the wetting on the solid wall is illustrated for six different snapshots. The liquid–liquid interface immediately forms a foot due to the boundary condition for the normal at the wall described above. The strong curvature in the foot region causes the fluid to move and the drop starts to wet the surface. The contact-line movement is fast in the initial steps but slows down as the drop approaches equilibrium. In Fig. 15 the change of the dynamic contact angle with time can be seen. The dynamic contact angle initially decreases rapidly with time but the decrease slows down as the angle approaches the equilibrium value.

In Fig. 16 the dynamic contact angle is plotted as a function of the Capillary number $\mathrm{Ca}^*=\frac{2\sqrt{2}\mu_{\mathrm{ref}}u}{3\sigma}=\frac{u}{u_{\mathrm{ref}}}$, which in this case is equal to the wetting speed. The results are compared with a phase field simulation [7] and Cox's theory [20]. The qualitative behavior of the simulation in this work is in agreement with previous results.

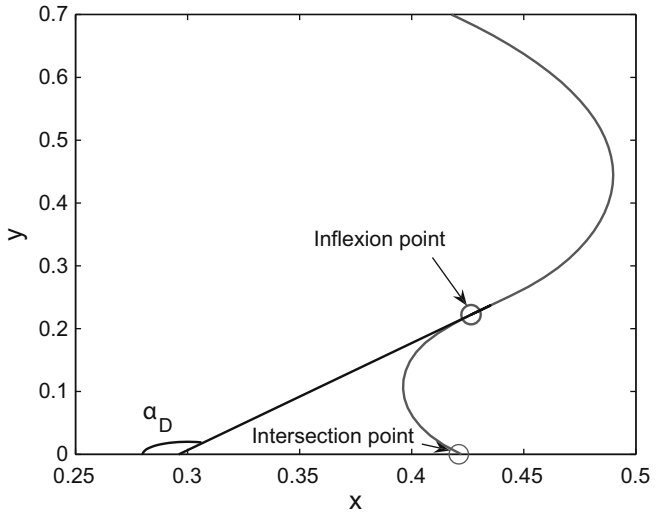

Fig. 13. The dynamic contact angle is measured by considering the tangent at the inflexion point. The wetting speed is given from the position of the intersection point at different times.

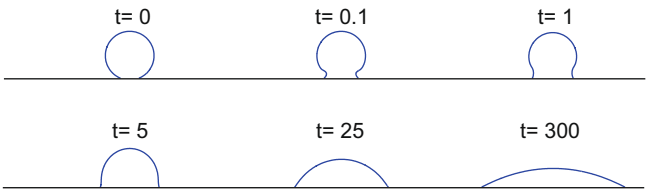

Fig. 14. Wetting of a liquid drop on a solid surface. The interface separating the two fluids at times $t = 0, 0.1, 1, 5, 25, 300$ with $\mathrm{Re} = 1, \mathrm{Ca} = 1$. The contact angles at the different times are $\alpha \approx 156, 149, 120, 88, 55, 27$.

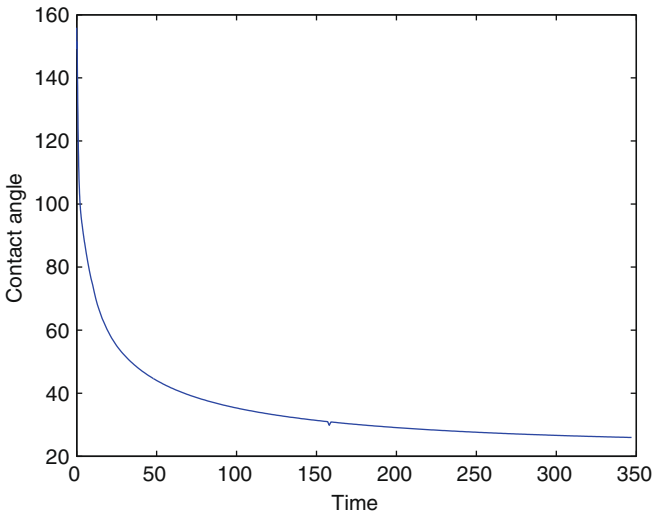

Fig. 15. Dynamic contact angle versus dimensionless time for a liquid droplet.

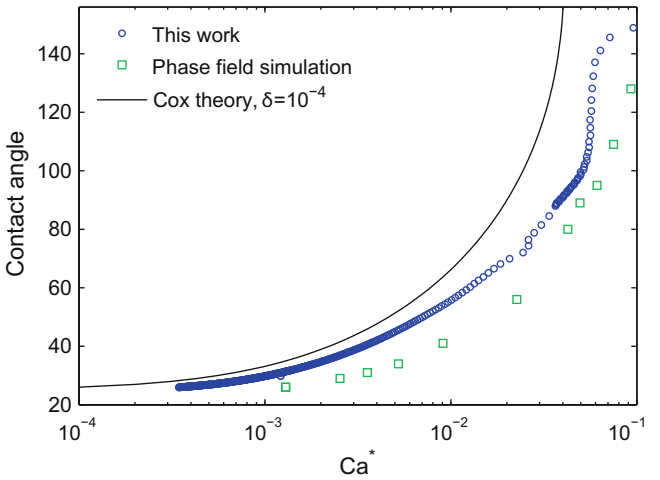

Fig. 16. The contact angle as a function of the capillary number. The initial angle is 156°. We compare the result of this work with the phase field simulation in [7] and Cox's theory [20]. The parameter δ in Cox's theory is chosen to be 10^{-4}, see Section 4.3.1.

4.4. Droplet on a flat plate – role of inertia

We consider here another two-dimensional droplet lying on a solid surface surrounded by another liquid with the same density and viscosity. The fluid is in rest and the configuration is in equilibrium except for the contact angle. The static contact angle is $\alpha_s = 70.53°$. The dimensionless parameters are Reynolds number $\mathrm{Re} = \frac{\rho_{\mathrm{ref}} u_{\mathrm{ref}} l_{\mathrm{ref}}}{\mu_{\mathrm{ref}}} = 20$ and the Capillary number $\mathrm{Ca} = \frac{\mu_{\mathrm{ref}} u_{\mathrm{ref}}}{\sigma} = 0.03$. In this example inertia plays an important role. Gravity effects are neglected. A simulation of this problem has previously been performed by Renardy et al. using a volume-of-fluid method [8].

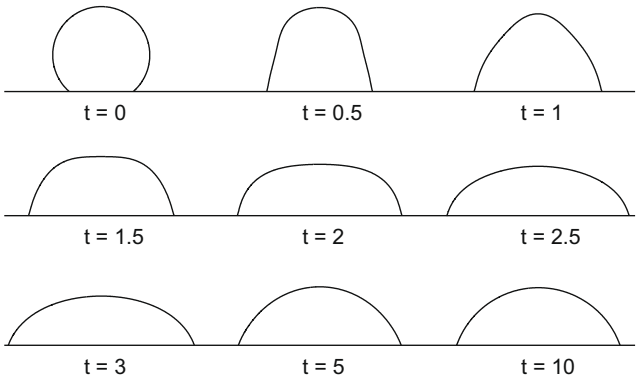

Fig. 17. Wetting of a liquid drop on a solid surface. The interface separating the two fluids at dimensionless times $t = 0, 0.5, 1, 1.5, 2, 2.5, 3, 5, 10$ with $\mathrm{Re} = 20, \mathrm{Ca} = 0.03$. The static contact angle $\alpha_s = 70.53$.

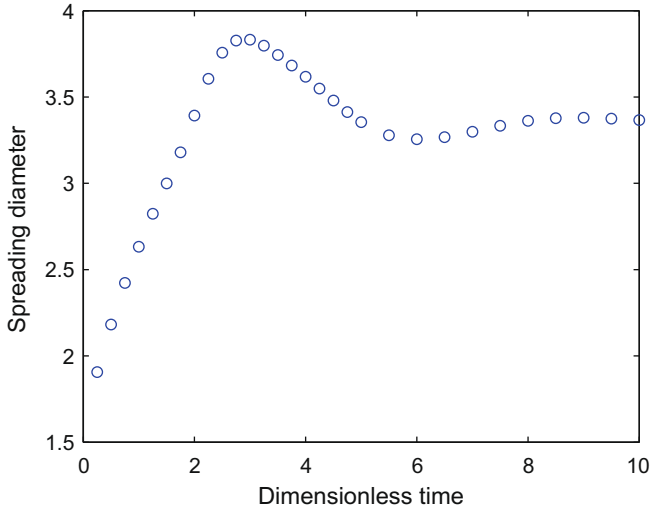

Fig. 18. Spreading diameter of the droplet in Fig. 17 as a function of dimensionless time. The drop oscillates towards equilibrium.

4.4.1. Computations

The computational domain is in non-dimensional coordinates $\{(x, y) : -3 \leqslant x \leqslant 3, 0 \leqslant y \leqslant 3\}$ and the initial drop is circular with non-dimensional radius $r = 1.0$ centered at $(x, y) = (0, 0.75)$. The simulation of the wetting is performed using a mesh consisting of regular triangles with 406×203 nodes and a time step $\Delta t = 10^{-4}$. In the reinitialization described in Eq. (12) the diffusion parameter in the normal direction is set to $\varepsilon_n = 3h$, where h is the mesh size, the diffusion parameter in the tangential direction is set to $\varepsilon_\tau = 3\varepsilon_n$, and the time step $\Delta\hat{t} = \Delta t$. In Eq. (11) giving the regularized normal vector field, the regularization parameter $\gamma = 2.5\varepsilon_n$.

In Fig. 17 the wetting on the solid wall is illustrated for nine different snapshots. The liquid–liquid interface starts to wet the surface because of the difference in the initial and the static contact angle. During the transient phase it passes the equilibrium position but then retracts and oscillates toward equilibrium. The snapshots can be compared with the snapshots from the volume-of-fluid computation in [8]. Note that, contrary to [8], the snapshots are in non-dimensional time. In Fig. 18, the spreading diameter, i.e. the distance between the two contact points, is plotted as a function of time. Note that this droplet oscillates toward equilibrium. This is because of the resistance of the drop to change its motion.

5. Discussion

We have developed and presented a conservative level set model for two-phase flow, which can capture contact line dynamics using no-slip boundary conditions for the velocity. In this model, which is an extension of the model presented in [11], the contact angle at equilibrium is used to induce a movement of the contact point by diffusion. In our model, a diffusion parameter and a regularization parameter are related to the size of the contact point region. Since the model is formulated in terms of partial differential equations on conservative form, conservation properties are retained by using standard conservative numerical methods.

Numerical computations for two different applications demonstrate that important features of contact line dynamics are captured. The results from the calculations of the droplets wetting walls have shown good agreement with other numerical methods and available theory. Parameter studies have indicated convergence as the model parameters approach their limit values. For cases when the mismatch in angle is moderate the method yields good results. For a fixed foot size, larger differences in angles would result in higher curvature and require a finer mesh in the foot region, making adaptive mesh refinement necessary. The refinement of the mesh could be based on the curvature.

In this work we have prescribed the static contact angle and have aimed to obtain an angle close to the static angle. In the first droplet on a flat plate calculation in Section 4.3, the difference between the initial and the prescribed static contact angle was large. Therefore, we had to choose between a large foot with the correct angle at the wall and a small foot but a larger discrepancy between the obtained angle and the prescribed static angle. We obtained much better results with a small foot region. The qualitative behavior was correct even though the small foot region resulted in a larger discrepancy between the obtained angle and the prescribed static angle. An important question is if the contact angle in computations has to be exactly equal to the static value. If it has to be equal, more tangential diffusion is needed. However, we do not want too much diffusion away from the foot region. Therefore, it could be beneficial to let the tangential diffusion vary with the distance from the contact point. We have performed numerical simulations with a tangential diffusion that decays exponentially with the distance from the boundary, and we have obtained promising results. This approach needs to be further investigated.

We have found that our method works well also in cases when the flow is not dominated by capillary forces, even without high resolution. For such cases it is not important that the interface attains the static angle at all times, only that the reinitialization procedure provides a mechanism for contact-line movement.

Acknowledgments

The authors acknowledge Gustav Amberg, Minh Do-Quang, and Emanuel Rubensson for helpful discussions on fluid dynamics, Femlego and numerics. This project has partially been financed by Swedish Foundation for Strategic Research (SSF), Center for Industrial and applied mathematics at KTH (CIAM), and Linné Flow center at KTH.

References

[1] R.M. German, Liquid Phase Sintering, Springer, 1985.
[2] P.G. deGennes, Wetting: statics and dynamics, Rev. Mod. Phys. 57 (1985) 827–863.
[3] T. Qian, Z.-P. Wang, P. Sheng, Molecular hydrodynamics of the moving contact line in two-phase immiscible flows, Commun. Comput. Phys. 1 (1) (2006) 1–52.
[4] L.M. Hocking, A moving fluid interface on a rough surface, J. Comput. Phys. 76 (1976) 801–817.
[5] P. Sheng, M. Zhou, Immiscible-fluid displacement: contact-line dynamics and the velocity-dependent capillary pressure, Phys. Rev. A 45 (1992) 5694.
[6] D. Jacqmin, Contact-line dynamics of a diffuse fluid interface, J. Fluid Mech. 402 (2000) 57–88.
[7] W. Villanueva, G. Amberg, Some generic capillary-driven flows, Int. J. Multiphase Flow 32 (2006) 1072–1086.
[8] M. Renardy, Y. Renardy, J. Li, Numerical simulation of moving contact line problems using a volume-of-fluid method, J. Comput. Phys. 171 (2001) 243–263.
[9] H. Liu, S. Krishnan, S. Marella, H. Udaykumar, Sharp interface cartesian grid method II: A technique for simulating droplet interactions with surfaces of arbitrary shape, J. Comput. Phys. 210 (2005) 32–54.
[10] E. Olsson, G. Kreiss, A conservative level set method for two phase flow, J. Comput. Phys. 210 (2005) 225–246.
[11] E. Olsson, G. Kreiss, S. Zahedi, A conservative level set method for two phase flow II, J. Comput. Phys. 225 (2007) 785–807.
[12] J. Sethian, Level Set Methods and Fast Marching Methods, Cambridge University Press, 1999.
[13] S. Osher, R. Fedkiw, Level Set Methods and Dynamic Implicit Surfaces, Springer-Verlag, 2003.
[14] A. Harten, The artificial compression method for computation of shocks and contact discontinuities, I. Single conservation laws, Commun. Pure Appl. Math. (1977) 611–638.
[15] J.-L. Guermond, L. Quartapelle, Calculation of incompressible viscous flows by an unconditionally stable projection FEM, J. Comput. Phys 132 (1997) 12–33.
[16] J.U. Brackbill, D. Kothe, C. Zemach, A continuum method for modeling surface tension, J. Comput. Phys 100 (1992) 335–353.
[17] A.-K. Tornberg, B. Engquist, A finite element based level set method for multiphase flow applications, Comput. Visualiz. Sci. 3 (2000) 93–101.
[18] M. Do-Quang, W. Villanueva, G. Amberg, I. Loginova, Parallel adaptive computation of some time-dependent materials-related microstructural problems, Bull. Polish Acad. Sci. 55 (2007) 229–237.
[19] R.L. Hoffman, A study of the advancing interface, J. Colloid Interface Sci. 50 (1975) 228–241.
[20] R.G. Cox, The dynamics of the spreading of liquids on a solid surface. Part 1, J. Fluid Mech. 168 (1986) 169–194.